H, He-like recombination spectra IV: clarification and refinement of methodology for l-changing collisions

N. R. Badnell[1], F. Guzmán[2⋆], S. Brodie[1], R. J. R. Williams[3], P. A. M. van Hoof[4], M. Chatzikos[2] and G. J. Ferland[2].
[1]Department of Physics, University of Strathclyde, Glasgow G4 0NG, UK
[2]Department of Physics and Astronomy, University of Kentucky, Lexington, KY 40506, USA
[3]Department of Physics and Astronomy, University of Leeds, Leeds LS2 9JT, UK
[4]Royal Observatory of Belgium, Ringlaan 3, 1180 Brussels, Belgium

Received

ABSTRACT
Precise spectral diagnostic modelling of H I and He II recombination spectra can constrain theoretical models which describe many astrophysical environments. Simple analytic expressions are of interest for collisional l-changing rate coefficients that are used by large-scale population modelling codes. We review, clarify and improve-upon the modified Pengelly & Seaton formulae of Guzmán et al. We show that the recent poor results for it shown by Vrinceanu et al. are due to their misinterpretation of its usage. We also detail efficient numerical algorithms which should enable the full quantum mechanical expression for such rate coefficients to be used much more routinely by modelling codes. We illustrate with some collisional-radiative population modelling for hydrogen.

Key words: atomic data – ISM: abundances – ISM: H II regions – cosmology: observations – primordial nucleosynthesis – radio lines

1 INTRODUCTION

Theoretical modelling of the observed recombination spectra of H I and He II (and some metals) is an important tool for predicting temperatures, densities, abundances (and more) of the local emitting/absorbing environment and thereby the testing of large-scale models of said environments. These range through gaseous nebulae (Osterbrock & Ferland 2006), H II regions (Anderson et al. 2018, Morabito et al. 2014), active galactic nuclei (Scotville & Murchikova 2013), the interstellar medium (Oonk et al. 2017) as well as the early universe (Izotov et al. 2007, 2014).

There has been an upsurge in interest in l-changing angular momentum collisions in recent years as ever greater precision is being demanded of spectral diagnostics. The capture-cascade problem is relatively straightforward to model. But heavy-particle collisions are efficient at changing the l-distribution of Rydberg atomic states during the cascade process and thus the intensity of lower-lying spectral diagnostic lines.

The seminal paper by Pengelly & Seaton (1964) used impact parameter theory to describe l-changing collisions. They provided simple analytic expressions for cross sections and rate coefficients for modelling use. All was quiet for half a century. Then Vrinceanu & Flannery (2001) analytically solved the time-dependent Schrödinger equation for a colliding heavy particle creating a weak electric field which lifts the Stark degeneracy in Rydberg atomic states. Comparison with quantum mechanical (QM) rate coefficients from this method showed that the simple expression of Pengelly & Seaton (1964) was not sufficiently accurate in extreme cases such as low temperatures (Guzmán et al. 2016) and/or for non-degenerate transitions (Guzmán et al. 2017).

Evaluation of the analytic quantum mechanical rate coefficients is rather demanding for modelling codes to carry-out routinely. Improved simple analytic expressions were sought. Guzmán et al. (2017) introduced a modified version of the Pengelly & Seaton (1964) approach which improved the description of close encounters (small impact parameters). Simple analytic expressions were resultant still which described both dense plasmas and non-degenerate transitions separately c.f. Pengelly & Seaton (1964). This is necessary because the dipole l-changing collision rate coefficients are logarithmically divergent unless an environmental cut-off is applied to the contribution from distant encounters (large impact parameters). The dense plasma (Debye) cut-off is independent of the collider energy but cut-offs due to non-degeneracy of a Rydberg transition or finite lifetime of the Rydberg state depend on the collider energy alone (Pengelly & Seaton 1964; Guzmán et al. 2017).

Vrinceanu et al. (2017, 2019) introduced a semi-classical (SC) approximation which gave an improved description at small impact parameters. The price to pay was in obtaining an analytic expression for the rate coefficient. Vrinceanu et al. (2019) provided one for the case of Debye cut-off. To do so requires that the de-

⋆ Present address: Department of Physics and Astronomy, University of North Georgia, Dahlonega, GA 30597, USA

scription of the collision problem does not depend independently on the impact parameter and collider energy. This enables a single (combined impact parameter/energy) analytic integration of the probability to be carried-out so as to deliver a rate coefficient. The combined dependency is true in principle but the introduction of an energy-dependent cut-off nullifies it. Energy-dependent cut-offs are important for non-hydrogenic targets and low-lying atomic p-states. The analytic modified Pengelly & Seaton rate coefficients of Guzmán et al. (2017) are required here. It is a concern then that Vrinceanu et al. (2019) appeared to obtain very poor results from the modified Pengelly & Seaton rate coefficients of Guzmán et al. (2017) for proton collisions with hydrogen.

In Section 2 we review, clarify and improve-upon the modified Pengelly & Seaton (PSM) method introduced by Guzmán et al. (2017). We show good accord between correctly interpreted PSM, semi-classical and quantum mechanical results in Section 3. We summarize our findings in Section 4. In Appendix A to this paper we detail the efficient numerical algorithms that we use to evaluate the quantum mechanical probabilities first formulated by Vrinceanu & Flannery (2001).

2 METHODOLOGY

Impact parameter theory (Alder et al. 1956) can be used to write the cross section σ_{ji} for an atomic transition $i \to j$ as

$$\sigma_{ji} = 2\pi \int_0^\infty P_{ji}(R) R \mathrm{d}R \tag{1}$$

in terms of the transition probability $P_{ji}(R)$ and impact parameter R.

The Bethe approximation can be used to write the probability for dipole transitions ($l \to l' = l \pm 1$) as

$$P_{ji}(R) = \frac{a_0^2 \mu I_\mathrm{H}}{2\omega_l E} \frac{D_{ji}}{R^2} \tag{2}$$

where E is the energy of the collider in units I_H, μ is the dimensionless reduced mass of the target–collider system, $\omega_l = 2l+1$ and a_0 is the Bohr radius.

The dipole factor D_{ji} for l-changing collisions (which is closely related to the atomic line strength) is given by

$$D_{ji} = \frac{Z^2}{z^2} 6 n^2 l_> (n^2 - l_>^2) \tag{3}$$

where Z is the charge of the collider, z is the charge of the target as seen by the Rydberg electron nl and $l_> = \max(l, l')$.

Energy-degenerate dipole transitions give rise to a logarithmic divergence in the cross section due to the contribution from distant encounters. The standard approach (Pengelly & Seaton, 1964) is to introduce a large impact parameter cut-off at R_c. The cut-off due to a finite density plasma neutralizing a Debye sphere is independent of the energy of the colliding particle. Finite lifetimes of the excited target-states and non-degenerate target energies for the transition clearly lead to a (collider) energy-dependent cut-off. The quantum mechanical (Vrinceanu & Flannery 2001) and semi-classical approximations of Vrinceanu et al. (2017, 2019) require such a cut-off as well.

Use of equation (2) also gives rise to a divergent probability as $R \to 0$. Pengelly & Seaton (1964) introduced a critical small impact parameter R_1 below which the probability was bounded: $P_{ji}(R < R_1) = P_1$ say. This completes the definition of the final-state resolved Pengelly & Seaton (1964) approximation. We denote it PS64.

It is well known that the PS64 approximation gives poor results and eventually breaks down for problems dominated by the contribution from small impact parameters such as low temperatures and/or high densities and/or severely non-degenerate transition energies.

Guzmán et al. (2017) introduced a modification of PS64 to overcome this limitation. It is based upon the behaviour of the quantum mechanical probability (Vrinceanu & Flannery, 2001; Vrinceanu et al. , 2012) at small impact parameters. They chose

$$P_{ji}(R < R_1) = P_1 \frac{R}{R_1} . \tag{4}$$

Combining (4) with equation (2) leads to the matching condition which defines R_1:

$$P_1 R_1^2 = \frac{a_0^2 \mu I_\mathrm{H}}{2\omega_l E} D_{ji} . \tag{5}$$

The cross section is then given by

$$\sigma_{ji}(E) = \pi P_1 R_1^2 \left[\frac{2}{3} + 2 \ln \left(\frac{R_\mathrm{c}}{R_1} \right) \right] \qquad \text{when } R_\mathrm{c} \geqslant R_1 \tag{6}$$

and by

$$\sigma_{ji}(E) = \pi P_1 R_1^2 \left(\frac{R_\mathrm{c}}{R_1} \right)^3 \frac{2}{3} \qquad \text{when } R_\mathrm{c} < R_1 . \tag{7}$$

The cross sections for $R_\mathrm{c} < R_1$ (equation 7) correspond with the scattering energies $E < E_\mathrm{min}$:

$$E_\mathrm{min} = \frac{a_0^2 \mu I_\mathrm{H}}{2 P_1 \omega_l R_\mathrm{c}^2} D_{ji} \tag{8}$$

which is defined by setting $R_1 = R_\mathrm{c}$ in equation (5). Cross sections at these energies are neglected by PS64. We denote this approximation PSM.

The corresponding rate coefficient q_{ji} at an electron temperature T_e is obtained by convoluting the cross section with a Maxwellian distribution over *all* collider energies. It takes on two forms.

(1) If the cut-off R_c is independent of the collider energy (e.g. Debye) then

$$q_{ji} = \frac{a_0^3}{\tau_0} \left(\frac{\pi \mu I_\mathrm{H}}{k_\mathrm{B} T_\mathrm{e}} \right)^{\frac{1}{2}} \frac{D_{ji}}{\omega_l} \left[\frac{\sqrt{\pi}}{2} U_\mathrm{m}^{-\frac{3}{2}} \mathrm{erf}(U_\mathrm{m}^{\frac{1}{2}}) - \mathrm{e}^{-U_\mathrm{m}}/U_\mathrm{m} + E_1(U_\mathrm{m}) \right] \tag{9}$$

where erf() denotes the error function, $E_1()$ the first exponential integral, $U_\mathrm{m} = E_\mathrm{min}/k_\mathrm{B} T_\mathrm{e}$, k_B the Boltzmann constant and τ_0 the Bohr time.

Guzmán et al. (2017) did not give this complete Debye form of the PSM rate coefficient since they were studying helium and so required the use of an energy dependent cut-off.

(2) The energy-dependent lifetime/splitting cut-off $R_\mathrm{c}(E) \propto \sqrt{E}$ will always be larger than the Debye one at sufficiently large collider energies. Guzmán et al. (2017) discuss how to split the convolution into two energy ranges $[0, E_\mathrm{c}]$ and $[E_\mathrm{c}, \infty)$ where the energy E_c is defined by $R_\mathrm{c}(E) = R_\mathrm{c}(\text{Debye})$. Thus

$$R_\mathrm{c}^2(E_\mathrm{c}) = \frac{E_\mathrm{c} t^2}{I_\mathrm{H} \mu} = \frac{k_\mathrm{B} T_\mathrm{e}}{8\pi a_0 I_\mathrm{H} N_\mathrm{e}} = R_\mathrm{c}^2(\text{Debye}) \tag{10}$$

and so

$$E_\mathrm{c} = \frac{\mu k_\mathrm{B} T_\mathrm{e}}{8\pi a_0 t^2 N_\mathrm{e}} . \tag{11}$$

Here N_e is the electron density (which defines the Debye sphere) and t is written in terms of the lifetime of the upper state (τ_{nl}) or in

Table 1. Comparison of He–p rate coefficients $q_{nl\to nl'}$ ($\mathrm{cm^3 s^{-1}}$) from the different theoretical PS, SC and QM methods for $n = 30$ and low- and high-l for different temperatures (T_H) at a hydrogen density N_H of 100 $\mathrm{cm^{-3}}$. QM-VOS12 denotes our use of the QM formula given in Vrinceanu et al. (2012); PS64 is the 'standard' Pengelly & Seaton (1964); PSM17 uses the original $P \propto R/R_c$ of Guzmán et al. (2017) when $R \leqslant R_\mathrm{c} \leqslant R_1$ while PSM20 uses the present $P \propto R/R_1$ instead; SC-VOS17 denotes the semi-classical method of Vrinceanu et al. (2017) and the results from which were not available to Guzmán et al. (2017).

		$N_\mathrm{H} = 100\ \mathrm{cm^{-3}}$		
		$T_\mathrm{H} = 10^2$K	$T_\mathrm{H} = 10^4$K	$T_\mathrm{H} = 10^6$K
$l = 4 \to l' = 3$	QM-VOS12	1.66[−3]†	5.61[+0]	3.51[+0]
	PS64	—	4.18[+0]	3.65[+0]
	PSM17	2.00[−2]	5.77[+0]	3.57[+0]
	PSM20	1.24[−3]	5.70[+0]	3.57[+0]
	SC-VOS17	1.91[−3]	6.25[+0]	3.94[+0]
$l = 29 \to l' = 28$	QM-VOS12	3.80[+1]	6.18[+0]	8.55[−1]
	PS64	4.06[+1]	6.44[+0]	8.81[−1]
	PSM17	3.80[+1]	6.18[+0]	8.54[−1]
	PSM20	3.80[+1]	6.18[+0]	8.54[−1]
	SC-VOS17	3.84[+1]	6.26[+0]	8.67[−1]

†1.66[−3] denotes 1.66×10^{-3}.

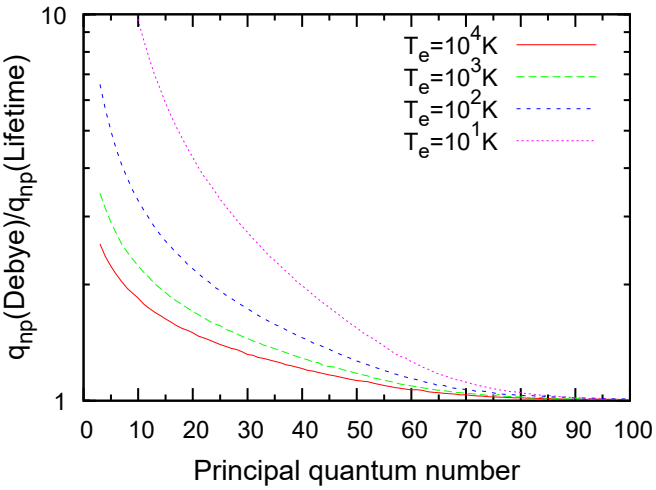

Figure 1. Ratio of PSM Debye-to-lifetime cut-off H–p rate coefficients $q_{n\mathrm{p}}$ at $T_\mathrm{e} = 10^1, 10^2, 10^3, 10^4$ K and $N_\mathrm{e} = 100\ \mathrm{cm^{-3}}$.

terms of the energy splitting (ΔE_{ji}) for the transition viz. $t = 0.72\tau_{nl}$ or $t = 1.12\hbar/\Delta E$ — see Pengelly & Seaton (1964), Guzmán et al. (2017).

The rate coefficient in this case is

$$q_{ji} = \frac{a_0^3}{\tau_0}\left(\frac{\pi\mu I_\mathrm{H}}{k_\mathrm{B}T_\mathrm{e}}\right)^{\frac{1}{2}}\frac{D_{ji}}{\omega_l} \times\left[4\left\{1-\mathrm{e}^{-\overline{U}_\mathrm{m}}\left(1+\overline{U}_\mathrm{m}+\tfrac{1}{2}\overline{U}_\mathrm{m}^2\right)\right\}\overline{U}_\mathrm{m}^{-3}+2E_1(\overline{U}_\mathrm{m})-E_1(U_\mathrm{c})\right] \quad (12)$$

where $\overline{U}_\mathrm{m}^2 = U_\mathrm{m}U_\mathrm{c}$ and $U_\mathrm{c} = E_\mathrm{c}/k_\mathrm{B}T_\mathrm{e}$. $E_1(U_\mathrm{c}\to\infty)\to 0$ applies the energy dependent cut-off at all energies. Note that this formula (12) assumes that $U_\mathrm{c} \geqslant \overline{U}_\mathrm{m}$. A more tedious expression results otherwise. We have yet to encounter its need.

Figure 1 shows the importance of applying a lifetime cut-off rather than a Debye cut-off for low-lying np states in H–p collisions.

Neither equation (12) nor equation (9) correspond quite with those discussed by Guzmán et al. (2017). The reason for this is that Guzmán et al. (2017) switched to using

$$P_{ji}(R) = P_1\frac{R}{R_c} \quad (13)$$

for $R \leqslant R_c \leqslant R_1$. This leads to

$$\sigma_{ji}(E\to 0) \sim E^0 \quad \text{or} \quad E^1 \quad (14)$$

for R_c(Debye) or $R_c(E)$ respectively.

Use of equation (4) still for $R \leqslant R_c \leqslant R_1$ leads to (see equations (5) & (7))

$$\sigma_{ji}(E\to 0) \sim E^{1/2} \quad \text{or} \quad E^2 \quad (15)$$

for R_c(Debye) or $R_c(E)$ respectively.

Study of the quantum mechanical cross sections at low energies does not yield an obvious verdict as to which to use. The asymptotic form does not appear to be reached until such low energies as to be irrelevant for temperatures > 1 K. The behaviour of the cross section at higher non-asymptotic energies likely dominates the practical application. There is some evidence from He–p collisions that the use of equation (4) is preferable still. In the present Table 1 we re-visit the He–p problem whose results were shown in Table 1 of Guzmán et al. (2017). The PSM results shown by Guzmán et al. (2017) broke down in the extreme case of a highly non-degenerate transition at low temperature. (We denote them PSM17.) The present results (which we denote PSM20) are of comparable accuracy to those we have obtained using the semi-classical approximation of Vrinceanu et al. (2017) and which were not available to Guzmán et al. (2017).

We return now to P_1 which bounds the probability for close encounters. We define generally

$$P_1 = \frac{1}{2}B_{ji} \quad (16)$$

where the branching ratio B_{ji} is given

$$B_{ji} = \frac{D_{ji}}{\omega_l D_{nl}} \quad (17)$$

and D_{nl} is the unresolved dipole quantity used by PS64

$$D_{nl} = \sum_{l'=l\pm1}\frac{1}{\omega_l}D_{ji} = \frac{Z^2}{z^2}6n^2(n^2-l^2-l-1)\,. \quad (18)$$

Guzmán et al. (2017) compared their PSM probabilities with the results that they obtained from the quantum mechanical approach of Vrinceanu & Flannery (2001) and detailed by Vrinceanu et al. (2012). Guzmán et al. (2017) chose

$$P_{\rm l} = \frac{1}{4}\,. \tag{19}$$

This is in contrast to Summers (1977) and Hummer & Storey (1987) who retained equation (16) to define their constant bound. The improvement on using equation (19) is marginal. We note that summing-over both final states leads in both cases to

$$P_{\rm l} = \frac{1}{2} \tag{20}$$

which is in agreement with Pengelly & Seaton (1964).

Comparison of the total collisional rate ($N_{\rm e}q_{nl}$) out of a state (nl) with the total radiative rate out (A_{nl}) is of interest in population modelling: $N_{\rm e}q_{nl}\tau_{nl} = 1$ defines the critical density above which $nl \rightarrow nl'$ collisions are faster than radiative ones ($\tau_{nl} = 1/A_{nl}$).

We have formulated l-changing collisions in a final-state resolved picture. One can simply sum over the final-state resolved rate coefficients

$$q_{nl} = \sum_{l'=l\pm1} q_{nl\rightarrow nl'} \tag{21}$$

to obtain a total unresolved rate coefficient. This is the only procedure available in the quantum mechanical case.

The problem was formulated historically in an unresolved picture — recall the original Pengelly & Seaton formula. Vrinceanu et al. (2019) consider an unresolved picture. By unresolved picture we mean that the matching point (e.g. R_1) in Pengelly & Seaton ($\pm$ modified) and the semi-classical approach of Vrinceanu et al. (2019) is defined in terms of the *total* probability out of nl. The modified Pengelly & Seaton $P_{nl\rightarrow nl-1}$ and $P_{nl\rightarrow nl+1}$ have *different* matching points in the resolved picture since we take $B_{ij} = 1/2$.

At this point it is worth recalling that the modified Pengelly & Seaton method was optimized for $nl \rightarrow nl-1$ transitions and data for $nl \rightarrow nl+1$ transitions should be determined from $nl \leftarrow nl+1$ via reciprocity e.g.

$$q_{nl} = q_{nl\rightarrow nl-1} + \frac{(2l+3)}{(2l+1)} q_{nl+1\rightarrow nl}\,. \tag{22}$$

This (application of reciprocity) is the normal procedure for evaluating all rates and rate coefficients when carrying-out population modelling so as to ensure one attains the LTE limit at high density.

The unresolved and resolved modified Pengelly & Seaton approaches should give similar results and increasingly so as the contribution from small impact parameters lessens. The contribution from small impact parameters becomes important at low temperatures and/or high densities. The original Pengelly & Seaton approach starts to fail here. The flexibility of using different resolved matching points may offer some improvement over the unresolved approach.

It is simple to deduce the modified Pengelly & Seaton formulae for the *unresolved* picture from the ones already given for the *resolved* picture:

1/ Replace B_{ij} by unity: **thus** $P_{\rm l} = 1/2$ **here** e.g. in Equ. (8).

2/ Replace D_{ji}/ω_l by D_{nl}.

We note that simply summing over the final-states in the resolved picture will yield (somewhat) different results to those obtained from using the explicit unresolved formulae of the modified Pengelly & Seaton approach. Both approaches require the evaluation of $\sim n$ expressions of similar complexity and so are similar in terms of computational effort.

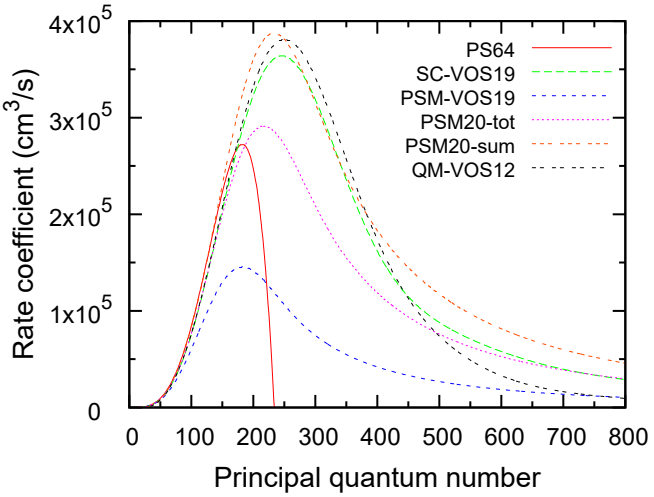

Figure 2. Total H–p rate coefficients q_{nl} for $n,l = 1$ at $T_{\rm e} = 10$ K and $N_{\rm e} = 100$ cm^{-3}. PS64 denotes the 'standard' Pengelly & Seaton (1964) method; SC-VOS19 denotes the semi-classical method of Vrinceanu et al. (2019); PSM-VOS19 denotes the modified Pengelly & Seaton method ($P_{\rm l} = 1/4$) of Vrinceanu et al. (2019); PSM20 denotes the present modified Pengelly & Seaton method ($P_{\rm l} = 1/2$); 'tot' denotes unresolved; 'sum' denotes resolved-sum (see text); QM-VOS12 denotes our use of the QM expressions given by Vrinceanu et al. (2012).

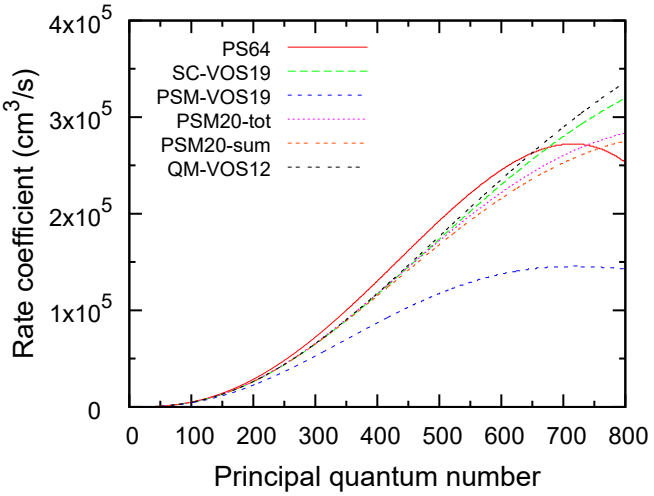

Figure 3. Total H–p rate coefficients q_{nl} for $n,l = n-2$ at $T_{\rm e} = 10$ K and $N_{\rm e} = 100$ cm^{-3}. PS64 denotes the 'standard' Pengelly & Seaton (1964) method; SC-VOS19 denotes the semi-classical method of Vrinceanu et al. (2019); PSM-VOS19 denotes the modified Pengelly & Seaton method ($P_{\rm l} = 1/4$) of Vrinceanu et al. (2019); PSM20 denotes the present modified Pengelly & Seaton method ($P_{\rm l} = 1/2$); 'tot' denotes unresolved; 'sum' denotes resolved-sum (see text); QM-VOS12 denotes our use of the QM expressions given by Vrinceanu et al. (2012).

3 RESULTS

All results shown in this section are calculated using the appropriate Debye cut-off unless stated otherwise.

Figure 2 compares total l-changing rate coefficients out of np states in hydrogen at an electron temperature of 10 K and density 100 cm^{-3}. A similar comparison was shown by Vrinceanu et al. (2019). They highlighted the poor agreement of the modified Pen-

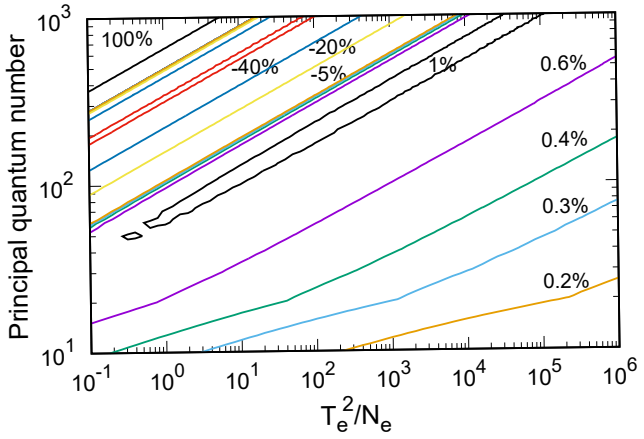

Figure 4. Percentage difference between PSM20-tot and QM-VOS12 total H–p rate coefficients q_{nl} for $n,l=1$ as a function of T_e^2/N_e. PSM20-tot denotes the present unresolved modified Pengelly & Seaton method; QM-VOS12 denotes our use of the QM expressions given by Vrinceanu et al. (2012).

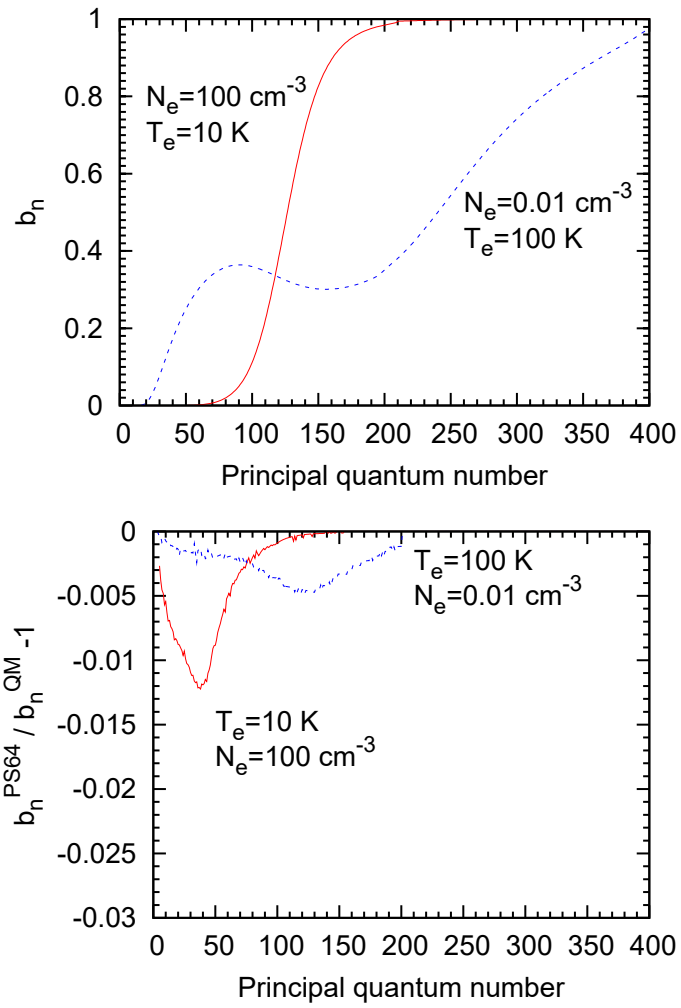

Figure 5. Hydrogen population modelling at $T_e=100$ K & $N_e=0.1$ cm^{-3} and $T_e=10$ K & $N_e=100$ cm^{-3}. Upper: departure coefficients b_n. The results for the present unresolved modified Pengelly & Seaton method (PSM20-tot), the original Pengelly & Seaton (1964) method (PS64) and our use of the QM expressions given by Vrinceanu et al. (2012) (QM-VOS12) are indistinguishable. Lower: fractional differences between PS64 and QM-VOS12 departure coefficients ($b_n^{PS64}/b_n^{QM}-1$). The differences between PSM20-tot and QM-VOS12 are not distinguishable from zero in this figure.

gelly & Seaton results (which we denote PSM-VOS19) with all other methods. This is due to the incorrect use by Vrinceanu et al. (2019) of $P_1=1/4$ for an unresolved transition. The correct results obtained using $P_1=1/2$ (which we denote PSM20-tot) are in much better accord. We note that we have not attempted to re-optimize the PSM R_1 matching point for this problem. Vrinceanu et al. (2019) re-optimized their matching point compared to Vrinceanu et al. (2017). Rather better agreement is found for PSM for n-values where the rate coefficient is largest if we sum-over the resolved rate coefficients (which we denote PSM20-sum). Figure 3 makes a similar comparison as Figure 2 but now for $n,l=n-2$. The results of all methods are in close accord except for the starkly different PSM-VOS19 ones.

Vrinceanu et al. (2019) present QM rate coefficients calculated at 15 n-values in their Figures 2(a) and 2(b). These correspond to our Figures 2 and 3. Vrinceanu et al. (2019) state that those QM rate coefficients for np took several hours of CPU time while those for $n,l=n-2$ took 2 days. We calculated our corresponding QM results at 800 n-values in less than 10s and 30s respectively. We detail in the Appendix the fast and efficient numerical algorithms that we have implemented. and which only require standard 64-bit floating point arithmetic. The algorithms used by Vrinceanu et al. (2019) required 400 digits of precision. The 5 orders of magnitude speed-up that we obtain with our algorithms means that their efficient implementation within modelling codes should make calculations using the QM method much more routine.

Figure 4 shows the percentage difference between our PSM20-tot results and the QM results (which we denote QM-VOS12) that we have computed using the expressions given by Vrinceanu et al. (2012). The comparison is again made for np states in hydrogen at an electron temperature of 10 K and density 100 cm^{-3}. We see that PSM20-tot is accurate to 1% or better over a wide range of the Debye temperature–density parameter space. This is in contrast to the few percent difference illustrated by Vrinceanu et al. (2019) for the original Pengelly & Seaton results (PS64). Vrinceanu et al. (2019) showed that their semi-classical results were also accurate to better than 1% over a similar range of parameter space — typically a factor 2 more accurate for a given temperature–density. All simple methods break-down rapidly at a critical and similar temperature–density diagonal ($T_e^2/(N_e n^4)$) as seen in Figure 4. The PSM results are well-behaved for all $T_e^2/(N_e n^4)$. They dip down and underestimate by up to 40% but ultimately end-up as a large overestimate compared to the QM rate coefficients. But the QM rate coefficients themselves are very large by then. Both sets of rates have already established a statistical l-population. Their magnitude is no longer relevant. Guzmán et al. (2016, 2017) provide illustrative figures for the H I and He I recombination spectra. All methods agree at low and high densities (excluding the original PS64).

We note that the results and timings for Figure 2 correspond to single vertical line in Figure 4. We have created and examined contour plots similar to those of Figure 4 but for $l=n/2$ and $l=n-2$. They all show a similar pattern. The results shown in Figure 4 are thus representative of the l-space as well.

We have carried-out population modelling with the spectral simulation code CLOUDY (Ferland et al. 2017). We used revision

r13930M on the PSM20 development branch of CLOUDY in which we have implemented the new equations given in Section 2. We again used the hydrogen-only-cloud model described by Guzmán et al. (2016). Figure 5 (upper) shows the thermal departure coefficients (b_n) at $T_e = 100$ K & $N_e = 0.1$ cm^{-3} and $T_e = 10$ K & $N_e = 100$ cm^{-3}. The b_n calculated using the PSM20-tot, PS64 and QM-VOS12 methods are indistinguishable in this figure. Figure 5 (lower) shows the corresponding fractional differences between PS64 and QM-VOS12 ($b_n^{\rm PS64}/b_n^{\rm QM} - 1$). The largest difference is $\sim 0.5\%$ and $\sim 1.2\%$ respectively for the two (T_e, N_e) cases. Vrinceanu et al. (2019) carried-out a similar comparison of their semi-classical results with the results of the original Pengelly & Seaton (1964) formula (PS64). The maximal differences were $\sim 0.8\%$ and $\sim 3.2\%$ for the same two cases. It should be noted that the two hydrogen models differ in their large-scale description (see Guzmán et al. (2016) and Vrinceanu et al. (2019) for details). The PSM20-tot fractional differences with QM-VOS12 are very small ($\sim 10^{-6}$) as are those for the original PSM17 approximation of Guzmán et al. (2017).

4 CONCLUSIONS

We have reviewed, clarified and improved-upon the modified Pengelly & Seaton PSM method introduced by Guzmán et al. (2017) which describes atomic l-changing collisions.

- We have shown that an alternative treatment of small impact parameters leads to much improved results from PSM in extreme cases such as highly non-degenerate transitions in He. We have provided complete expressions for rate coefficients for both an energy independent (Debye) cut-off at large impact parameters (see equation (9)) as well as for (collider) energy-dependent cut-offs due to non-degenerate transitions and/or finite atomic lifetimes (see equation (12)). The latter is not available for the semi-classical approach of Vrinceanu et al. (2017, 2019).
- We have pointed-out the mis-interpretation made by Vrinceanu et al. (2019) when they adapted the final-state resolved PSM approach of Guzmán et al. (2017) to the unresolved case. Correct interpretation leads to good accord between PSM results and those we have obtained using their semi-classical (Vrinceanu et al. 2019) and quantum mechanical (Vrinceanu & Flannery 2001) methods.
- We have described the numerical algorithms that we use to evaluate the quantum mechanical probabilities (see Appendix A). They are many orders of magnitude faster than those described by Vrinceanu et al. (2019) and they only require the use of standard 64-bit floating point arithmetic. Their efficient implementation within modelling codes should make such calculations much more routine.

5 DATA AVAILABILITY

Results shown in the Figures will be shared on reasonable request to the corresponding author.

The Fortran codes which implement the algorithms described in Appendix A are available from the UK APAP Network website: apap-network.org. This includes a library of Wigner 3n-j programs (at apap-network.org/3n-j) and a test-driver/wrapper-plus-subprogram to calculate the QM and PSM20 Maxwellian rate coefficients (at apap-network.org/lchng). The programs are interactive and should be self-explanatory.

6 ACKNOWLEDGEMENTS

NRB acknowledges support from STFC (UK) through the University of Strathclyde APAP Network grant ST/R000743/1. FG and GJF acknowledge support from the National Science Foundation (grant number 1816537) and NASA ATP program (grant number 17-ATP17-0141). MC acknowledges support by NSF (1910687), NASA (19-ATP19-0188), and STScI (HST-AR-14556.001-A).

7 REFERENCES

Alder K., Bohr A., Huus T., Mottelson B., Winther A., 1956, Rev.Mod.Phys., 28, 432
Abramowitz M., Stegun I. A., 1972, *Handbook of Mathematical Functions* Dover, NY
Anderson L. D., Armentrout W. P., Luisi M., Bania T. M., Balser D. S., Wenger T. V., 2018, ApJS, 234, 33
Edmonds A. R., 1957 *Angular Momentum in Quantum Mechanics* Princeton, NJ
Ferland G. J., Chatzikos M., Guzmán F., Lykins M. L., van Hoof P. A. M., Williams R. J. R., Abel N. P., Badnell N. R., Keenan F. P., Porter R. L., Stancil P. C., 2017 Rev.Mex.Astron.Astrofis., 53, 385
Guzmán F., Badnell N. R., Williams R. J. R., van Hoof P. A. M., Chatzikos M., Ferland G. J., 2016 MNRAS, 459, 3498
Guzmán F., Badnell N. R., Williams R. J. R., van Hoof P. A. M., Chatzikos M., Ferland G. J., 2017 MNRAS, 464, 312
Guzmán F., Chatzikos M., van Hoof P. A. M., Blaser D. S., Dehghanian M., Badnell N. R., Ferland G. J., 2019 MNRAS, 486, 1003
Izotov Y. I., Thuan T. X., Stasifińska G., 2007, ApJ, 662, 15
Izotov Y. I., Thuan T. X., Guseva N. G., 2014, MNRAS, 445, 778
Luscombe J. H., Luban M., 1998, Phys.Rev.E, 57, 7274
Morabito L. K., Oonk J. B. R., Salgado F., Toribio M. C., Röttergering H. J. A., Tielens A. G. G. M., Beck R., Adebahr B., Best P., Beswick R., Bonafede A., Brunetti G., Brüggen M., Chyży K. T., Conway J. E., van Driel W., Gregson J., Haverkorn M., Heald G., Horellou C., Horneffer A., Iacobelli M., Jarvis M. J., Marti-Vidal I., Miley G., Mulcahy D. D., Orrú E., Pizzo R., Scaife A. M. M., Varenius E.,van Weeren R. J., White G. J., Wise M. W., 2014, ApJ, 795, L33
Oonk J. B. R., van Weeren R. J., Salas P., Salgado F., Morabito L. K., Toribio M. C., Tielens A. G. G. M., Röttergering H. J. A., 2017, MNRAS, 465, 1066
Osterbrock D.E., Ferland G.J., 2006, Astrophysics of gaseous nebulae and active galactic nuclei, 2nd ed. University Science Books, Sausalito, CA
Pengelly R. M., Seaton M. J., 1964, MNRAS, 127, 165
Racah G., 1942, Phys.Rev., 62, 438
Schulten K., Gordon R. G., 1975a, J.Math.Phys., 16, 1961
Schulten K., Gordon R. G., 1975b, J.Math.Phys., 16, 1971
Schulten K., Gordon R. G., 1976, Comput.Phys.Commun., 11, 269
Scoville N., Murchikova L., 2013, ApJ, 779, 75
Summers H. P., 1977, MNRAS, 178, 101
Vrinceanu D., Flannery M. R., 2001, Phys.Rev.A 63, 032701; J.Phys.B, 34, L1
Vrinceanu D., Onofrio R., Sadeghpour H. R., 2012, ApJ, 747, 56
Vrinceanu D., Onofrio R., Sadeghpour H. R., 2017, MNRAS, 471, 3051
Vrinceanu D., Onofrio R., Oonk J. B. R., Salas P., Sadeghpour H. R., 2019, ApJ, 879, 115

APPENDIX A: NUMERICAL ALGORITHMS FOR THE QUANTUM MECHANICAL APPROACH

The quantum mechanical impact parameter probability of Vrinceanu & Flannery (2001) can be written (Vrinceanu et al. 2012)

$$P_{ji}(R) = (2l'+1)\sum_{L=|l-l'|}^{n-1}(2L+1)\left\{\begin{array}{ccc} l' & l & L \\ j & j & j \end{array}\right\}^2 \quad \text{(A1)}$$
$$\times\frac{(L!)^2(n-L-1)!}{(n+L)!}(2\sin\chi)^{2L}\left[C_{n-L-1}^{(L+1)}(\cos\chi)\right]^2$$

where $j=(n-1)/2$ and $C_n^{(\gamma)}$ denotes an ultraspherical (or Gegenbauer) polynomial. The rotation angle χ between the orientation of the initial- and final-states is given by

$$\cos\chi = \frac{1+\alpha^2\cos(\pi\sqrt{1+\alpha^2})}{1+\alpha^2} \quad \text{(A2)}$$

for straight-line trajectories. The scattering parameter α is given by

$$\alpha = \frac{3Zn}{2vzR} \quad \text{(A3)}$$

where v denotes the speed of the collider.

Evaluation of both the ultraspherical polynomials and the $6j$-symbols $\{\ldots\}$ is numerically challenging on considering principal quantum numbers up to ~ 1000 and for all allowed orbital angular momenta due to under- & over-flow and cancellation error. Vrinceanu et al. (2019) used high precision (400 digits) to overcome this but note that it took 2 days of CPU time on a single processor machine to evaluate the QM results of Figure 3. We describe the algorithms that we use for their evaluation and which are many orders of magnitude faster since they require only standard 64-bit floating point arithmetic for example.

Quadrature: We remark in passing that we evaluate all probability integrals using the trapezoidal rule utilizing a logarithmic α-mesh. This simultaneously yields both cross sections and rate coefficients.

A1 Ultraspherical Polynomials

We describe a fast, accurate and stable algorithm for the evaluation of ultraspherical polynomials $C_n^{(\gamma)}(x)$ as they occur in (A1).

We exploit the fact that $\gamma+n$ is fixed in the summation. Use Abramowitz & Stegun (22.7.3):

$$(n+1)C_{n+1}^{(\gamma)}(x) = 2(n+\gamma)xC_n^{(\gamma)}(x) - (n+2\gamma-1)C_{n-1}^{(\gamma)}(x) \quad \text{(A4)}$$

to eliminate $C_{n+1}^{(\gamma)}$ from Abramowitz & Stegun (22.7.23):

$$(n+\gamma)C_{n+1}^{(\gamma-1)}(x) = (\gamma-1)\left[C_{n+1}^{(\gamma)}(x) - C_{n-1}^{(\gamma)}(x)\right] \quad \text{(A5)}$$

to obtain

$$(n+1)C_{n+1}^{(\gamma-1)}(x) = 2(\gamma-1)\left[xC_n^{(\gamma)}(x) - C_{n-1}^{(\gamma)}(x)\right]. \quad \text{(A6)}$$

Then use (A4) again to eliminate $C_{n-1}^{(\gamma)}$ from (A5) so as to obtain

$$(n+2\gamma-1)C_{n-1}^{(\gamma)}(x) = 2\gamma\left[C_{n-1}^{(\gamma+1)}(x) - xC_{n-2}^{(\gamma+1)}(x)\right] \quad \text{(A7)}$$

on relabelling $n\to n-2$ and $\gamma\to\gamma+1$.

Initialize $C_{-1}^{(\gamma)}(x)=0$ and $C_0^{(\gamma)}(x)=1$. Then equations (A6) and (A7) can be used in tandem to make a single pass recurrence synchronized with the summation in (A1) which must start at the upper limit here. The equations (A6) and (A7) are coupled directly here through the $C_{n-1}^{(\gamma)}(x)$ terms.

The above algorithm is applicable up to principal quantum number $n\approx 650$ using 64-bit floating point arithmetic. Simply rescaling $C_0^{(\gamma)}(x)$ once extends the use of 64-bit arithmetic up to $n\approx 1500$ without the need to resort to higher precision. This is sufficiently high in n so as to establish collisional LTE.

A2 Wigner $6j$-symbols

Racah (1942) first gave a closed expression for the recoupling of three angular momenta to give a resultant total — the Racah W-coefficient — which is written in terms of factorials. These factorials can become rather large in practical applications and so subject to cancellation error and under- & over-flow when evaluated numerically. The Wigner $6j$-symbol is closely related to the Racah W-coefficient but it exhibits the full symmetry of the problem (Edmonds 1957).

Consider the evaluation of the $6j$-symbol

$$\left\{\begin{array}{ccc} a & b & c \\ d & e & f \end{array}\right\}. \quad \text{(A8)}$$

Define

$$w(j) = \left\{\begin{array}{ccc} j & b & c \\ d & e & f \end{array}\right\} \quad \text{(A9)}$$

where b,c,d,e,f have been specified already. Any $6j$-symbol can be re-ordered thus. The $w(j)$ satisfy the following linear 3-term recurrence relation (Edmonds 1957, Schulten & Gordon 1975a):

$$jA(j+1)w(j+1) + B(j)w(j) + (j+1)A(j)w(j-1) = 0 \quad \text{(A10)}$$

for $j_{\min}\leqslant j\leqslant j_{\max}$ where $j_{\min}=\max\{|b-c|,|e-f|\}$ and $j_{\max}=\min\{|b+c|,|e+f|\}$.

The $A(j)$ and $B(j)$ correspond to specific $6j$-symbols with an argument $1/2$. They are given by

$$\begin{aligned} A(j)^2 &= [j^2-(b-c)^2][(b+c+1)^2-j^2] \\ &\times [j^2-(e-f)^2][(e+f+1)^2-j^2] \end{aligned} \quad \text{(A11)}$$

and

$$\begin{aligned} B(j)/(2j+1) &= j(j+1)[-j(j+1)+b(b+1)+c(c+1)] \\ &+ e(e+1)[j(j+1)+b(b+1)-c(c+1)] \\ &+ f(f+1)[j(j+1)-b(b+1)+c(c+1)] \\ &- 2j(j+1)d(d+1)]. \end{aligned} \quad \text{(A12)}$$

Note that $A(j_{\min})=0=A(j_{\max}+1)$. A two-term relation then starts-off the unnormalized recurrence. The solution is subsequently normalized via

$$\sum_j (2j+1)(2d+1)\left\{\begin{array}{ccc} j & b & c \\ d & e & f \end{array}\right\}^2 = 1. \quad \text{(A13)}$$

The phase is determined through

$$\text{sign}\left\{\begin{array}{ccc} j & b & c \\ d & e & f \end{array}\right\} = (-1)^{b+c+e+f}. \quad \text{(A14)}$$

The above linear 3-term recurrence relation (A10) can be viewed as a finite-difference relation for a second-order differential equation c.f. the Schrödinger equation for a bound-state electron. It suffers a similar pathology to its solution.

We note that the range $j_{\min} \leqslant j \leqslant j_{\max}$ can be further subdivided as

$$j_{\min} \leqslant j \leqslant j_{\rm I} \leqslant j \leqslant j_{\rm II} \leqslant j \leqslant j_{\max} \tag{A15}$$

where $j_{\rm I} \leqslant j \leqslant j_{\rm II}$ defines the classically-allowed region of $w(j)$ and where the solution is oscillatory as a function of j. This region corresponds to the resultant j following the coupling of 3 angular momenta. These boundaries $j_{\rm I}$ and $j_{\rm II}$ (corresponding to the turning points $w''(j) = 0$) can be determined from the root of a Cayley determinant (Schulten & Gordon 1975b).

The required solution for $w(j)$ is exponentially decreasing in the classically-forbidden regions $j_{\min} \leqslant j \leqslant j_{\rm I}$ and $j_{\rm II} \leqslant j \leqslant j_{\max}$ as $j \to j_{\min}$ and $j \to j_{\max}$. The recursion must then start at both ends and match somewhere in the classically-allowed region so as to avoid picking-up the complementary exponentially increasing solution. Note that the use of a linear 3-term recurrence relation in the classically-forbidden region leads to the need for constant rescaling so as to avoid both numerical under- and over-flow.

The algorithm detailed above has been implemented by Schulten & Gordon (1976) as the CPC program ACWQ.

The use of a non-linear 2-term recurrence relation in the classically-forbidden region avoids the need for continual rescaling (Luscombe & Luban 1998). Define

$$r(j) \equiv \frac{w(j)}{w(j-1)}\,. \tag{A16}$$

Then the original recurrence relation (A10) can be written as

$$r(j) = \frac{-(j+1)A(j)}{B(j) + jA(j+1)r(j+1)} \quad \text{for} \quad j \leqslant j_{\max} - 1\,. \tag{A17}$$

This defines a backwards recurrence with starting value

$$r(j_{\max}) = -(j_{\max}+1)A(j_{\max})/B(j_{\max}) \tag{A18}$$

since $A(j_{\max}+1) = 0$. Then $w(j)$ for $j_{\rm II}+1 \leqslant j \leqslant j_{\max}$ is given by

$$w(j_{\rm II}+k) = w(j_{\rm II}) \prod_{p=1}^{k} r(j_{\rm II}+p) \tag{A19}$$

for $1 \leqslant k \leqslant j_{\max} - j_{\rm II}$. The value of $w(j_{\rm II})$ at this point is both undefined and arbitrary.

This approach avoids under- and over-flow issues since $r(j)$ is bounded above by order unity. One can extend the evaluation somewhat into the classically-allowed region but must stop short of $w(j)$ changing sign so as to ensure that $w(j) \neq 0$.

Now define

$$s(j) \equiv \frac{w(j)}{w(j+1)}\,. \tag{A20}$$

Then the original recurrence relation (A10) can be written as

$$s(j) = \frac{-jA(j+1)}{B(j) + (j+1)A(j)s(j-1)} \quad \text{for} \quad j \geqslant j_{\min} + 1\,. \tag{A21}$$

This defines a forwards recurrence with starting value

$$s(j_{\min}) = -j_{\min}A(j_{\min}+1)/B(j_{\min}) \tag{A22}$$

since $A(j_{\min}) = 0$. Then $w(j)$ for $j_{\min} \leqslant j \leqslant j_{\rm I} - 1$ is given by

$$w(j_{\rm I}-k) = w(j_{\rm I}) \prod_{p=1}^{k} s(j_{\rm I}-p) \tag{A23}$$

for $1 \leqslant k \leqslant j_{\rm I} - j_{\min}$. The value of $w(j_{\rm I})$ is again both undefined and arbitrary.

We now need to determine $w(j)$ in the classically-allowed region and match with the arbitrary/undefined $w(j_{\rm I})$ and $w(j_{\rm II})$. Define

$$w_{\rm I}(j) \equiv \frac{w(j)}{w(j_{\rm I})} \quad \text{and} \quad w_{\rm II}(j) \equiv \frac{w(j)}{w(j_{\rm II})}\,. \tag{A24}$$

These quantities $w_{\rm I}(j)$ and $w_{\rm II}(j)$ satisfy the original 3-term recurrence relation. It is well-behaved in the classically-allowed region.

Use the initial values $w_{\rm I}(j_{\rm I}-1) = s(j_{\rm I}-1)$ and $w_{\rm I}(j_{\rm I}) = 1$ so as to carry-out a forwards recurrence for $w_{\rm I}(j)$ starting at $j = j_{\rm I}$ and on out to $j = j_m \leqslant j_{\rm II}$. Use the initial values $w_{\rm II}(j_{\rm II}+1) = r(j_{\rm II}+1)$ and $w_{\rm II}(j_{\rm II}) = 1$ so as to carry-out a backwards recurrence for $w_{\rm II}(j)$ starting at $j = j_{\rm II}$ and on in to $j = j_m \geqslant j_{\rm I}$. Then we have that

$$\frac{w_{\rm II}(j_m)}{w_{\rm I}(j_m)} = \frac{w(j_m)}{w(j_{\rm II})} \times \frac{w(j_{\rm I})}{w(j_m)} = \frac{w(j_{\rm I})}{w(j_{\rm II})}\,. \tag{A25}$$

We see that our two unknowns $w(j_{\rm I})$ and $w(j_{\rm II})$ are reduced to a single unknown (ratio).

We have $w_{\rm II}(j)$ over $j_m \leqslant j \leqslant j_{\rm II}$. We obtain the remaining values for $j_{\rm I} \leqslant j \leqslant j_m$ from

$$w_{\rm II}(j) = w_{\rm I}(j) \times \frac{w(j_{\rm I})}{w(j_{\rm II})}\,. \tag{A26}$$

We now have $w(j)$ over $j_{\rm I} \leqslant j \leqslant j_{\rm II}$:

$$w(j) = w_{\rm II}(j) w(j_{\rm II}) \tag{A27}$$

in terms of the unknown factor $w(j_{\rm II})$. This factor can be determined through use of the normalization condition (A13). Then $w(j_{\rm I})$ can be determined from (A25). We already have $w(j)$ in the classically forbidden region where it is written in terms of $w(j_{\rm I})$ and $w(j_{\rm II})$ — see (A19) and (A23). This completes the determination of the $w(j)$.

The algorithm described above for the determination of $6j$-symbols is accurate for pathological cases such as

$$\left\{ \begin{array}{ccc} 170/2 & 168/2 & 172/2 \\ 179/2 & 179/2 & 179/2 \end{array} \right\} = 3.3988213869 \times 10^{-8} \tag{A28}$$

for which cancellation is an issue unless high precision is used. There are no issues with regards to over/underflow. These again require high precision or constant re-scaling when using other algorithms. We note that a $6j$-symbol with a value of $\lesssim 10^{-16}$ is indistinguishable from being identically zero in the classically-allowed region when using 64-bit floating point arithmetic. We set such to zero.

We remark that this approach for $6j$-symbols can be adapted easily for the calculation of $3j$-symbols as well (c.f. Schulten & Gordon 1975a).